RSC Advances

PAPER

View Article Online
View Journal | View Issue

Cite this: *RSC Adv.*, 2020, **10**, 25446

Novel huperzine A based NMDA antagonists: insights from molecular docking, ADME/T and molecular dynamics simulation studies †

Dilep Kumar Sigalapalli,[a] Raghu Rangaswamy[b] and Neelima D. Tangellamudi *[a]

Received 23rd January 2020
Accepted 7th May 2020

DOI: 10.1039/d0ra00722f

rsc.li/rsc-advances

Huperzine A (**HupA**) is an alkaloidal natural product and drug isolated from Chinese herb *Huperzia serrata*, which is a potent selective anticholinesterase inhibitor. **HupA** has symptomatic, cognitive-enhancing and protective effect on neurons against amyloid beta-induced oxidative injury and antagonizing *N*-methyl-D-aspartate receptors by blocking the ion channels. The present study aimed to identify the docking, ADME/T and molecular dynamics simulation parameters of a library of 40 analogues which can correlate the binding affinity, conformational stability and selectivity of the ligands towards NMDA receptor through *in silico* approach. Glide molecular docking analysis was performed for the designed analogues to understand the binding mode and interactions. MD simulations were performed to explain the conformational stability and natural dynamics of the interaction in physiological environmental condition of protein–ligand complex affording a better understanding of chemical-scale interactions between **HupA** and its analogues with NMDA channel that could potentially benefit the development of new drugs for neurodegenerative diseases involving NMDA receptors.

1. Introduction

Alzheimer's disease (AD) is predicted to reach epidemic proportions, with an enormous human and economic burden, by the year 2050. Alzheimer's is a type of dementia that causes problems with memory, thinking and behavior and other cognitive abilities that interfere with daily life.[1,2] Thus effective therapies that prevent AD or slow its progression or treat its cognitive and behavioral symptoms are urgently needed to avert this public health crisis.[3,4] Several advances have been made recently to understand the neurobiology of AD. The major known cause for progression of disease is oligomerization of amyloid beta (Aβ) which is formed from amyloid precursor protein (APP) by the action of beta secretase and gamma secretase.[5,6] An increased production of Aβ oligomers leads to synaptic depression and a reduced capacity for synaptic plasticity.[7–9] Several studies have shown that a blockade of *N*-methyl-D-aspartate receptors (NMDARs) can mitigate the effects of Aβ on synapses.[10–12] NMDARs are involved in learning and memory function in the CNS and play a major role in the synaptic plasticity.[13–15] NMDARs can both promote neuronal protection and kill neurons depending on its site of location. Specifically NMDARs which are present in synaptic region promote neuronal protection. In contrast, activation of NMDARs which are localized at extrasynaptic region produces neuronal death.

NMDARs have been identified into different subtypes such as GluN1, GluN2A, GluN2B, GluN2C, GluN2D, GluN3A and GluN3B. NMDARs are hetero-tetramers associated with two GluN1 and two GluN2 subunits.[16] GluN1 is gated by glycine, whereas GluN2 is gated by glutamate. Recent results indicate that Aβ oligomers increase the GluN2A to GluN2B ratio by selectively reducing the synaptic currents of GluN2B-containing NMDARs. Such a GluN2B to GluN2A switch also requires an alternative NMDAR function that involves glutamate-binding to GluN2B leading to conformational changes of the GluN2B-NMDAR, but does not involve ion flux through the NMDAR.[17] This ion flux-independent glutamate binding to GluN2B leads to synaptic loss and an ultimate neuronal death. Hence selective GluN2B antagonists can be designed to target the amyloid beta induced dysfunction.[18]

NMDA receptor antagonists play a significant role for the treatment AD disease. Huperzine A (**HupA**) is an alkaloidal natural product isolated from chinese herb *Huperzia serrata*, which is a potent selective anticholinesterase inhibitor with antioxidant and neuroprotective properties. The availability of **HupA** from natural sources is scarce and trivial modifications on **HupA**, thus far, have led to less effective analogues. State Food and Drug Administration of China approved huperzine for Alzheimer's treatment in 1994. Earlier reports demonstrate that **HupA** is an inhibitor of NMDA receptors as well, with good

[a]*Department of Medicinal Chemistry, National Institute of Pharmaceutical Education and Research (NIPER), Hyderabad 500037, India. E-mail: neelima.niperhyd@gov.in; tdneelima@gmail.com*

[b]*Department of Bioinformatics, Alagappa University, Karaikudi – 630 003, Tamil Nadu, India*

† Electronic supplementary information (ESI) available. See DOI: 10.1039/d0ra00722f

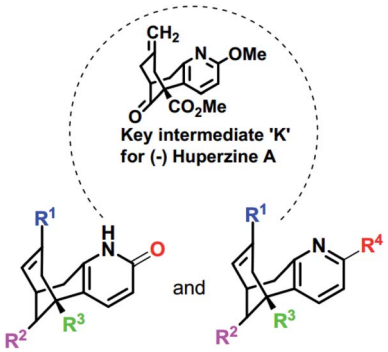

Scheme 1 Skeletal structures of the molecules designed based on K [I–X and NM (1–30)]. The structures of designed analogues of K are furnished in ESI Fig. S4.†

efficacy in enriching memory in various animal models.[19,20] **HupA** is proved to be a non-competitive NMDA antagonist, which inhibits the NMDA-induced toxicity by blocking ion channels of NMDA receptor through binding at **MK-801** binding site.[21] The scarcity of **HupA** from natural sources induced several groups to develop synthetic routes to this compound and its numerous analogues as cholinesterase inhibitors. The reported structures represent rather trivial and obvious modifications to the parent structure and were found to be either less effective than **HupA** by the *in silico* or *in vitro* studies.[22–25] We surmised that more "creative" alterations of **HupA** will provide more active analogues, and thus we have designed some novel analogues based on the structure of the key intermediate for **HupA** serving as a starting point, in the present study.[26–29] As per these previous reports, the key intermediate for **HupA**, '**K**' could be obtained by asymmetric palladium catalyzed bicycloannulation of a β-keto ester. Thus we have designed the analogues I–X and NM (1–30) with subtle manipulation of the functionalities on the key intermediate **K** with a future focus to possibly obtain the analogues by simple chemical transformations of **K** (Scheme 1). In consequence, our present investigations are directed towards the design and *in silico* studies of the designed analogues to explore the ligand–enzyme interactions (Scheme 1).

2. Materials and methods

2.1 Rationale of work

To the best of our knowledge, molecular modeling studies were not explored either on **HupA** or its analogues as NMDA receptor antagonists. Recently, Song X. *et al.* solved the crystal structure of heterotetrameric GluN1/GluN2B NMDA receptor which proved the mechanistic inhibition of NMDA receptor by **MK-801** *via* ion channel blocking.[30] This gave an encouraging start to our computational exploration in identifying some of the synthetically possible **HupA** analogues as NMDA receptor antagonists. In the present work, we have designed novel compounds with basic skeleton cycloocta[*b*]pyridine structural framework of the **HupA**. Fig. 1 demonstrates the schematic version of the present work. The demands of this endeavor of designing and discovering efficient NMDA receptor antagonists were met by structural variations derived from the biologically viable functionalities that were visualized and carefully incorporated on the structure of the key intermediate **K**. Molecular docking simulation studies were conducted to examine the detailed protein–ligand interactions between the active site of NMDA receptor and the designed molecules. ADME/T prediction studies enabled us understand the drug-likeliness of the designed molecules, while molecular dynamics simulation studies explained the natural dynamics of interaction in physiological conditions, of the top potential hits among the designed molecules as NMDA receptor antagonist.

2.2 Computational methods

2.2.1 Selection of target protein. To the best of our knowledge, the crystal structure for GluN1/GluN2B NMDA receptor of humans with good resolution has not been reported yet. The crystallographic structures of *Xenopus laevis* GluN1/GluN2B NMDA receptor (PDB ID 5UN1) were selected for

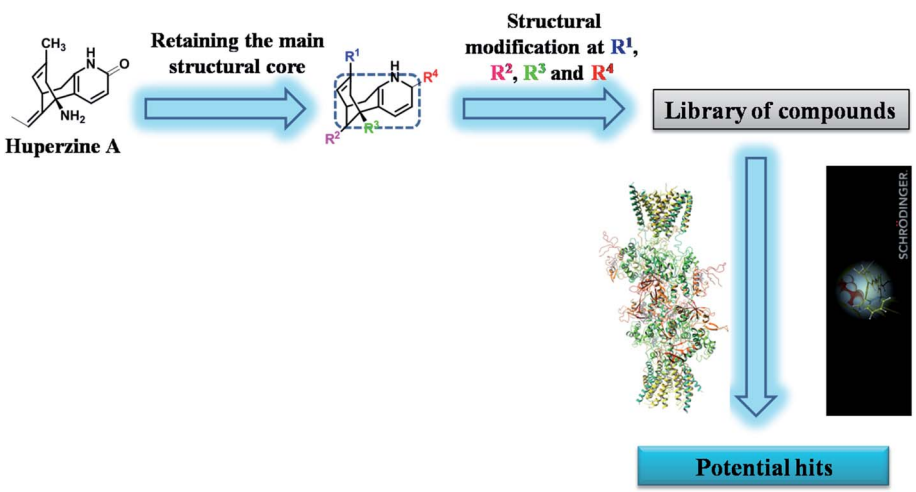

Fig. 1 Schematic representation of the research protocol in the present study.

further studies. The protein sequence of *Homo sapiens* GluN1 (Uniprot, Entry Id: Q05586) and GluN2B (Uniprot, Entry Id: Q13224) was downloaded from the Universal Protein Resource. Further, targeted heterotetrameric GluN1/GluN2B NMDA protein search was performed using Blast Search tools against the PDB databank. Structure prediction wizard tool of Maestro was used for comparative analysis of *Homo sapiens* and *Xenopus laevis* NMDA receptor protein sequence.[31] Fig. S1 and S2 (ESI)† demonstrate 92.1% and 82.6% identity in the protein sequence alignment of GluN1 and GluN2B from *Homo sapiens* with those from *Xenopus laevis*, respectively.

2.2.2 Protein structure preparation. The coordinates for the NMDA receptor were downloaded from the RCSB protein data bank (PDB ID 5UN1). The protein structure was processed using the Protein Preparation Wizard (PPW) and its integrity was checked and adjusted by adding the missing residues by employing Prime module of Schrödinger suite.[32,33] The water molecules and all other heteroatoms were removed from the protein crystal structure. The H-bond network was optimized and the overlapping hydrogens were fixed under the refine tab of PPW. The most likely positions of thiol and hydroxyl hydrogen atoms, protonation states and tautomers of various amino acid residues were selected by the protein assignment script shipped by Schrodinger. The pH range was set to 7.0 and the protein was minimized by applying OPLS_2005 force field. Finally, restrained minimization was performed until the average root mean square deviation (RMSD) of the non-hydrogen atoms converged to 0.30 Å.

2.2.3 Identification of binding sites on NMDA receptor using SiteMap analysis. The prepared NMDA receptor was further subjected to SiteMap computer program to identify their potential binding sites. SiteMap combines a novel and highly effective algorithm for rapid binding site identification for various proteins.[34,35] Table S1 (ESI)† depicts the SiteMap analysis results for top most potential binding sites of NMDA receptor. Site-I of NMDA receptor was found to possess the top most Site score (ligand binding ability) and D score (druggability). The size and volume of Site-I binding site is admirable. Hydrophobic (hydrophobic character of the binding site) score of Site-I is convincingly excellent. Fig. S3 (ESI)† illustrates the identified potential binding site (Site-I) on NMDA receptor. Site-I also covers the specific active site residues present at **MK-801** binding site. Visualization and characterization of the catalytic binding site was done using the SiteMap module of Maestro 11.1. Further, preparation of the receptor grid for target protein was done utilizing OPLS_2005 force field. The grid center was set to be the centroid of the active site, and the size of the cubic grid was fixed at 20 Å.

2.2.4 Ligand preparation. A total of 40 molecules were built on Maestro Molecule Builder of Schrödinger and optimized using OPLS_2005 force field in LigPrep module of Schrödinger software 2017-1.[36] All the possible protomers and ionization states were enumerated for ligands at a pH of 7.4 using Ionizer. The tautomeric states were generated for chemical groups with possible prototropic tautomerism.

2.2.5 Molecular docking. Molecular docking studies were performed by using GLIDE (Grid-based Ligand Docking with Energetics) docking module of Schrödinger suite, wherein, the prepared ligands were docked into the generated receptor grid using Glide SP docking precision.[37,38] It uses a grid-based ligand docking method with energetic, that searches for favorable interactions between a ligand and a receptor molecule like protein. Van der Waals scaling factor and partial charge cutoff was selected to be 0.80 and 0.15, respectively for ligand atoms. The interactions of each complex were analyzed and the 3D poses demonstrating the molecular recognition interactions were obtained using Schrödinger suite 2017-1 and PyMOL v0.99.[39]

2.2.6 *In silico* physico-chemical and ADME/T studies. Physico-chemical and ADME/T properties, which help in predicting both physico-chemical significant descriptors and pharmacokinetically important properties of the molecules, were calculated using Qikprop module of Schrödinger suite 2017-1.[40] QikProp enumerates the comparative ranges of a molecule's properties with those of known drugs. Major parameters of the designed molecules that enabled us to quickly evaluate the physico-chemical and ADME/T properties of designed **HupA** analogues are discussed in Section 3.2.

2.2.7 Molecular dynamics. In order to understand the dynamic interaction mechanism between the receptor and the ligand, we have performed molecular dynamics simulation study using Desmond module of Schrödinger suite 2017-1.[41] Aqueous biological system was built by using OPLS_2005 force field and TIP3P model was used to stimulate the water molecules. Orthorhombic periodic boundary conditions were set up to specify the shape and size of the repeating unit buffered at 10 Å distances. Boundary conditions box volume was initially calculated as 2 223 364 $Å^3$ (for 5UN1–**HupA** complex); 2 223 334 $Å^3$ (for 5UN1–**MK-801** complex); 2 223 382 $Å^3$ (for 5UN1–**NM28** complex) and then minimized to 2 136 731 $Å^3$, 2 136 683 $Å^3$ and 2 136 758 $Å^3$ respectively. Required number of sodium and chloride ions was added to neutralize the system and osmotic effect of water was maintained by adding 0.15 mol L^{-1} sodium and chloride ions. After building the solvated system containing protein in complex with the ligand, the system was minimized and relaxed using default protocol integrated within Desmond module using OPLS_2005 force field parameters. 300 K temperature and 1 atmospheric pressure were maintained by using Nose–Hoover temperature coupling and isotropic scaling, respectively. Reversible reference system propagation algorithm (REPSA), a time stepping algorithm was used for far non-bonded, near non-bonded and bonded interactions (6, 2 and 2 fs, respectively) and finally, the molecular dynamics simulations (100 ns) were performed by using Desmond module of Schrödinger suite.

3. Results and discussion

3.1 Molecular docking study

Molecular docking studies were performed to elucidate the binding mode and type of interactions for designed **HupA** analogues at the active site of NMDA receptor (PDB ID 5UN1) using GLIDE docking module of Schrödinger suite 2017-1. To validate the docking protocol, the bound ligand (**MK-801**) was

Table 1 GLIDE docking results for some of the designed HupA analogues at the active site of NMDA receptor (PDB ID 5UN1)

S. no.	Ligand name	Ligand structure	Docking score	Hydrophobic interactions
1	**Huperzine A**	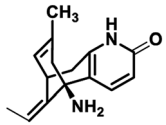	−6.970	Met631(A), Val634(A), Ala635(A), Phe597(B), Leu626(B), Ala627(B), Tyr629(B), Val634(C), Ala635(C), Ala622(D), Val623(D), Leu626(D), Ala627(D)
2	**NM14**	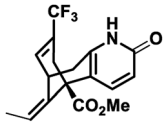	−7.475	Met631(A), Val634(A), Ala635(A), Phe597(B), Val623(B), Leu626(B), Ala627(B), Tyr629(B), Val634(C), Val623(D), Leu626(D), Ala627(D)
3	**NM16**	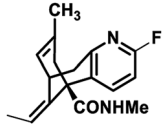	−7.542	Met631(A), Val634(A), Ala635(A), Leu626(B), Ala627(B), Tyr629(B), Val634(C), Ala635(C), Val623(D), Leu626(D), Ala627(D), Ala631(D)
4	**NM20**	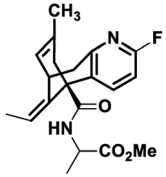	−7.722	Met631(A), Val634(A), Ala635(A), Val623(B), Leu626(B), Ala627(B), Tyr629(B), Val634(C), Ala622(D), Val623(D), Leu626(D), Ala627(D)
5	**NM22**	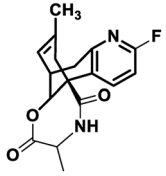	−7.558	Met631(A), Val634(A), Ala635(A), Val623(B), Leu626(B), Ala627(B), Val634(C), Ala635(C), Val623(D), Leu626(D), Ala627(D)
6	**NM28**	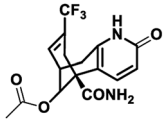	−7.830	Val634(A), Phe597(B), Val623(B), Leu626(B), Val634(C), Val623(D), Leu626(D), Ala627(D)
7	**MK-801**	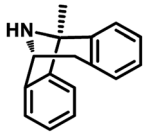	−7.365	Met631(A), Val634(A), Ala635(A), Leu626(B), Ala627(B), Tyr629(B), Val623(D), Leu626(D), Ala627(D)

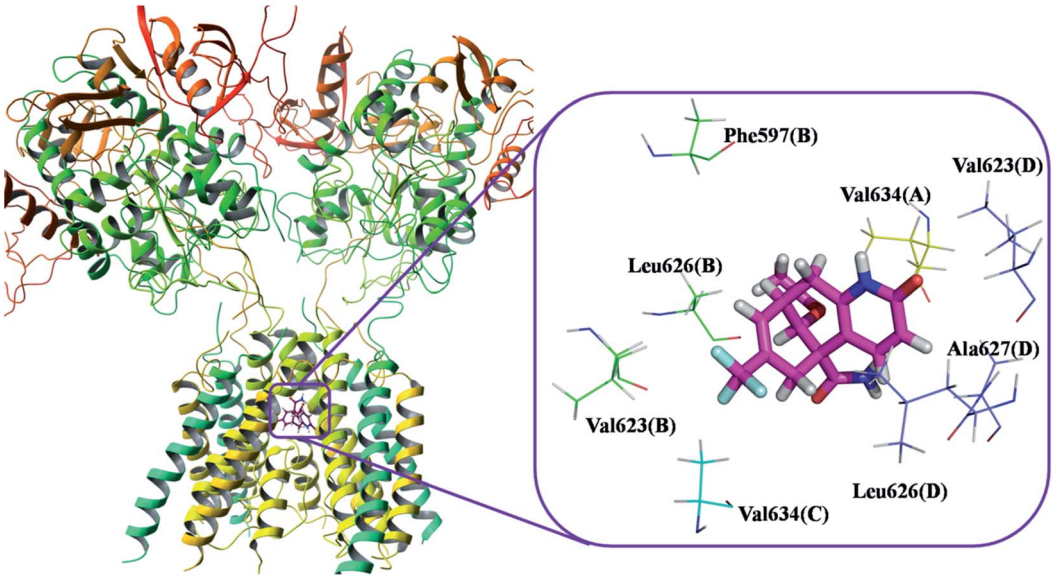

Fig. 2 Binding pose and detailed protein interaction of the most potent NM28 (magenta colour stick) with NMDA receptor. All the amino residues represent hydrophobic interactions.

extracted from the prepared protein structure and was re-docked, after which the RMSD was determined. After validation of the docking protocol, the **HupA** analogues were docked into the active site of NMDA receptor.

This molecular docking simulation study suggested that the top ranked conformations of **HupA** analogues were well lodged at the active binding site of NMDA receptor. Table 1 showed the results of docking along with the major interactions for some of

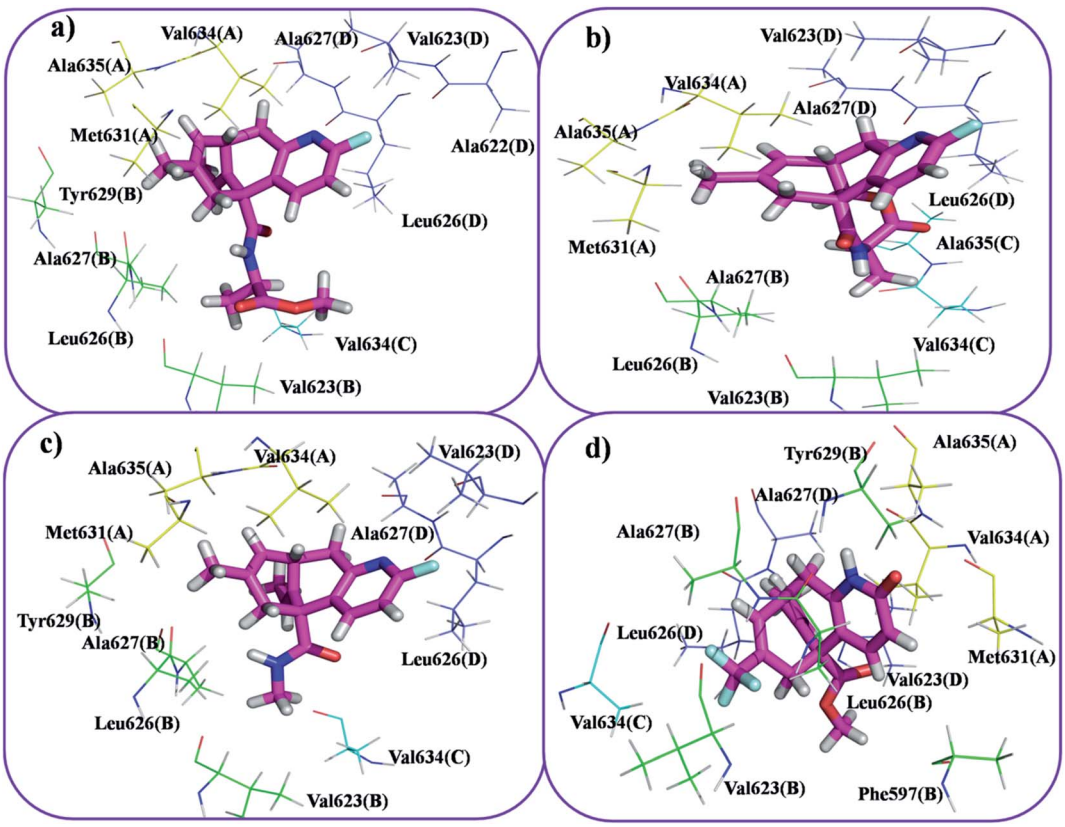

Fig. 3 Docking model of compound NM20 (a), NM22 (b), NM16 (c) and NM14 (d) with NMDA receptor. All the amino residues represent hydrophobic interactions.

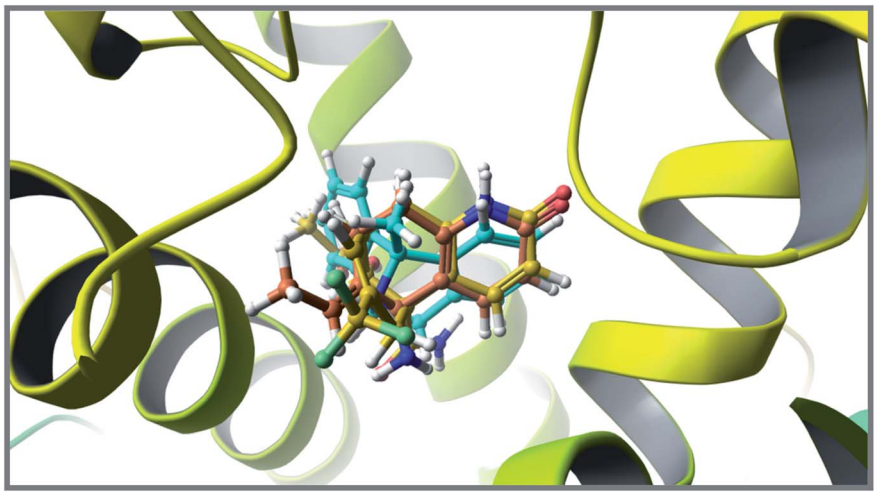

Fig. 4 Superimposition of co-crystallized ligand (turquoise), HupA (orange) and best docked pose of NM28 (yellow) at the active site of NMDA receptor.

the designed **HupA** analogues with NMDA receptor with scores above −7.4, which is higher than that of the co-crystal. Interestingly, out of all the designed **HupA** analogues, **NM28** was found to possess higher interaction energy (−7.830 kcal mol^{-1}) than the co-crystalized ligand and **HupA**. Fig. 2 shows binding pose and detailed protein interaction of **NM28** within the active site of NMDA receptor. Several hydrophobic interactions observed between the **NM28** and the active site residues, such as Val634(A), Phe597(B), Val623(B), Leu626(B), Val634(C), Val623(D), Leu626(D) and Ala627(D) stabilize the binding of the **NM28** in the binding site of NMDA receptor. Further, compounds **NM14**, **NM16**, **NM20** and **NM22** showed good interaction energy with target NMDA receptor *i.e.* −7.475 kcal mol^{-1}, −7.542 kcal mol^{-1}, −7.722 kcal mol^{-1}, and −7.558 kcal mol^{-1}, respectively. Fig. 3 demonstrates the docking model of compounds **NM14**, **NM16**, **NM20** and **NM22** at the binding site of NMDA receptor. Superimposition of native ligand, **HupA** and best docked pose of **NM28** at the active pocket of NMDA receptor is depicted in Fig. 4, which reveals that **NM28** and **HupA** share a common binding pattern with **MK-801**. Pyridin-2-one ring of the **NM28** and **HupA** overlap with one of the benzene ring of iminodibenzo annulene of **MK-801**. The docking analysis, revealed good hydrophobic contacts of designed **HupA** analogues with all the four chains of heterotetrameric GluN1/GluN2B NMDA receptor, which may be responsible for the selective blockade of ion channel. Thus, the molecular docking results, allow us to believe that some of the **HupA** analogues have potential to inhibit NMDA receptor through an action on binding site.

3.2 *In silico* ADME/Tstudies

The drug likeliness of the designed **HupA** analogues was evaluated in terms of the physicochemically important descriptors and key pharmacokinetic properties through the QikProp program of Schrödinger software. The lead molecules obtained from docking study (Fig. 5) were subjected for QikProp ADME/T profiling. Some of the computed ADME/T parameters are shown in Table 2. From this *in silico* study, we can compare the ADME/T properties of the known NMDA receptor channel blockers and our designed molecules.

The lead molecules of **HupA** based designed library showed significant values for the properties analyzed and on the basis of physico-chemical properties, they exhibited drug-like characteristics. ADME/T prediction studies depicts that the designed **HupA** analogues conform to the Lipinski's rule of five. They have appropriate log *P* values for desired biological efficacy and showed no violation in the recommended ranges of physico-chemical and ADME/T parameters. The other associated factors, such as blood–brain permeability and percent human oral absorption are also within the acceptable range defined for human use. Interestingly from this study we have observed compound **NM28** to possess highest polar surface area amongst the designed **HupA** analogues, indicating the drug likeness of the designed **HupA** analogues.

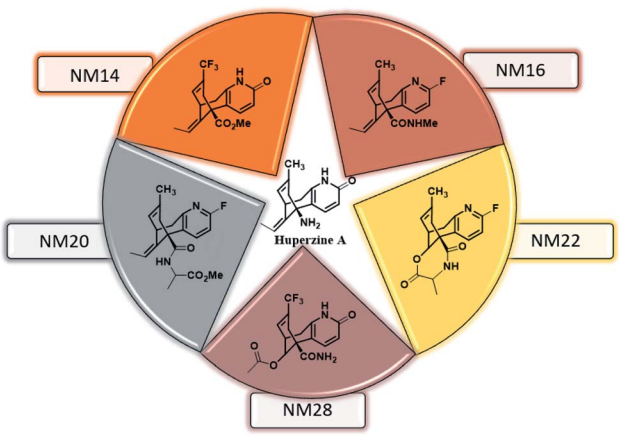

Fig. 5 Structures of the lead molecules.

Table 2 Physico-chemical properties and ADME/T profile of designed HupA analogues[a]

	Parameters						
Compound name	Rule of five	PSA	QP log $P_{o/w}$	QP_{polrz}	QP log BB	QP log K_p	POA
NM14	No violation	71.606	3.384	34.117	−0.343	−3.340	100.000
NM16	No violation	43.172	3.184	32.668	0.184	−1.947	100.000
NM20	No violation	73.086	3.861	39.674	−0.207	−2.230	100.000
NM22	No violation	81.467	1.469	33.519	−0.463	−3.421	81.681
NM28	No violation	123.117	0.857	32.679	−1.123	−4.762	64.640
Huperzine A	No violation	63.754	1.466	27.760	−0.156	−5.346	75.744
MK-801	No violation	15.003	3.310	27.642	0.770	−2.947	100.000

[a] PSA = polar surface area, QP log $P_{o/w}$ = predicted octanol/water partition coefficient, QP_{polrz} = predicted polarizability, QP log BB = predicted brain/blood partition coefficient, QP log K_p = predicted skin permeability, POA = predicted human oral absorption.

3.3 Molecular dynamics simulation

From the molecular docking analysis, the best docked complexes were extracted to explore the conformational stability and time dependent performance of the ligands at the active pocket of NMDA receptor. Molecular docking predicts the spatial orientation of a ligand in the active pocket of the receptor. Subsequently, in addition to the fit of the binding pocket, other factors such as binding affinity and conformational stability should be taken into consideration for the development of compounds targeting NMDA receptor in the treatment of Alzheimer's disease. Conformational stability is crucially important for potent inhibition of NMDA receptors and an MD study provides conformational landscape of ligand–protein complexes at given temperature. The molecular dynamics simulation (MD) were performed for protein–ligand complex of compound **NM28**, **MK-801** and **HupA** using Desmond module of Schrödinger suite 2017-1.

Molecular dynamics trajectory was used to examine the equilibration of dynamics over period of time. An insight about the convergences of simulated protein–ligand complexes can be obtained by taking into consideration the root-mean-square deviations (RMSD) of initial structure and average simulated structure of all the frames in MD trajectory. Configuration RMSD of all the selected complexes with respect to their initial structures were found to increase and then converge after 20 ns during equilibration phase. Initially, RMSD of the C-alphas, heavy atoms, backbone and side chains during MD simulation of **NM28**–5UN1 complex shows little fluctuations, but during course

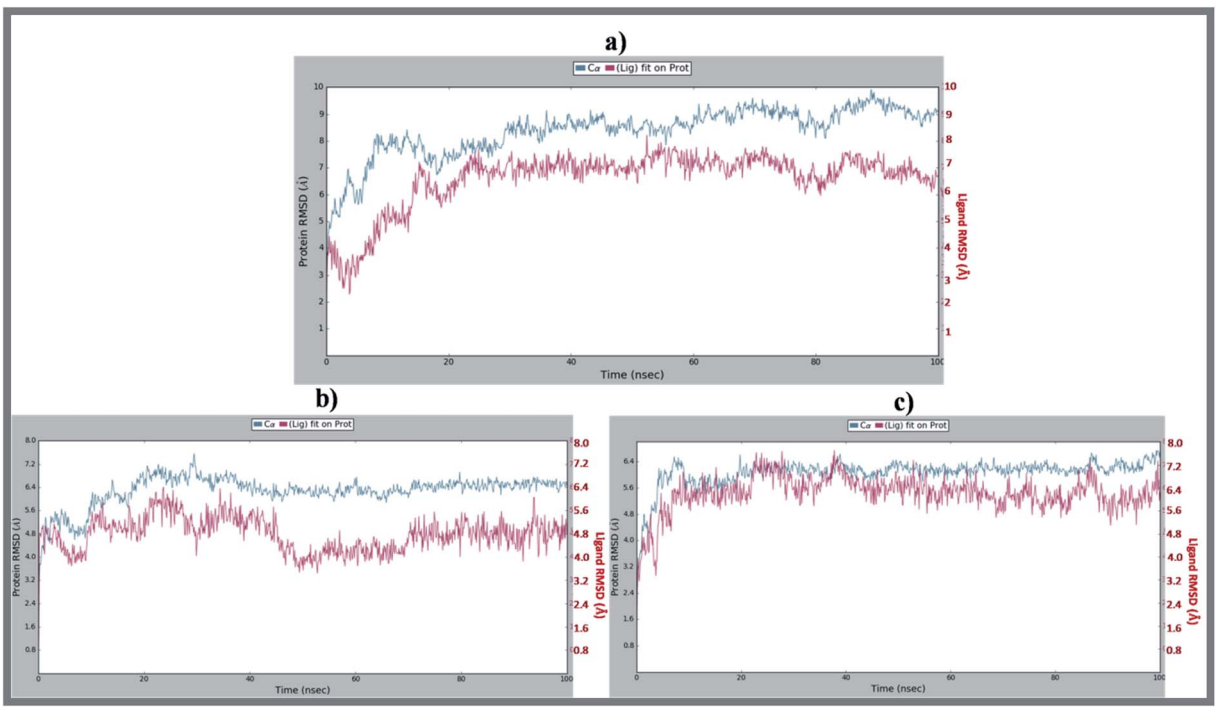

Fig. 6 Average RMSD of C-alphas of protein and ligand complexes (a) **NM28**–5UN1, (b) **MK-801**–5UN1 and (c) **HupA**–5UN1 during molecular dynamics simulation (100 ns).

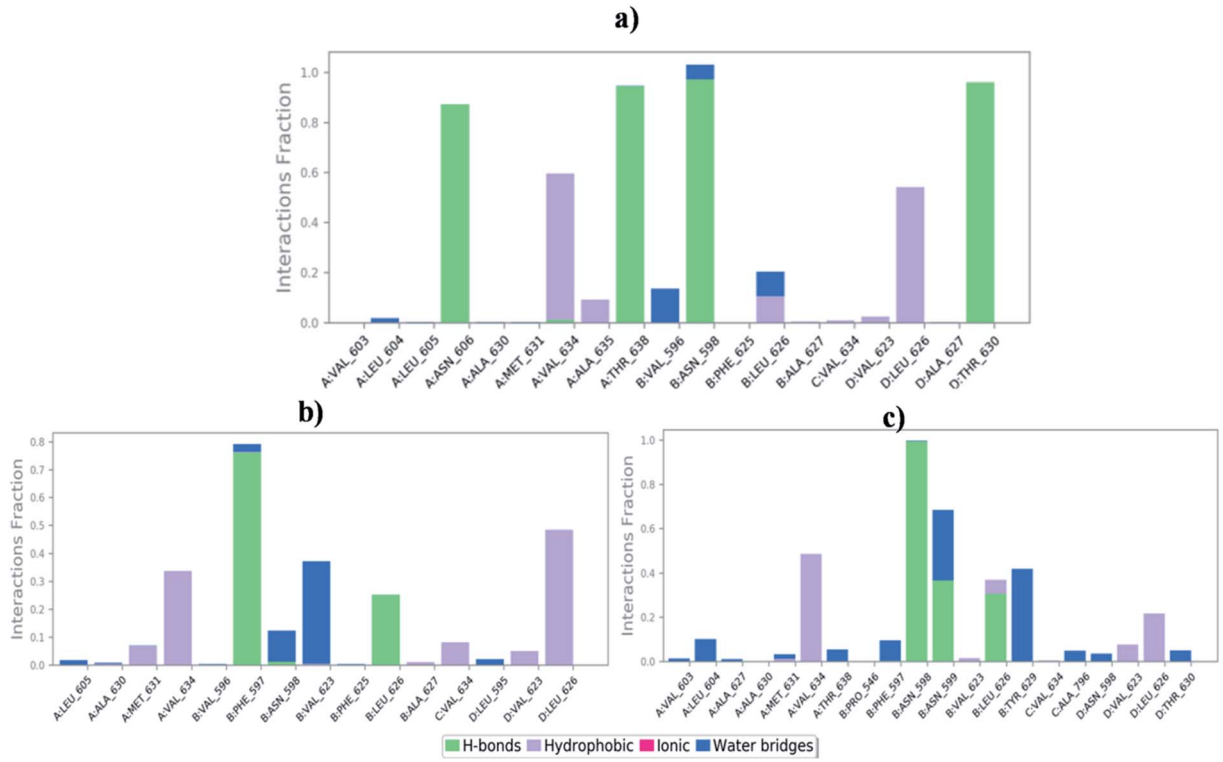

Fig. 7 Bar-chart representation of protein–ligand contacts of (a) **NM28**–5UN1 complex, (b) **MK-801**–5UN1 complex and (c) **HupA**–5UN1 complex during molecular dynamics simulation.

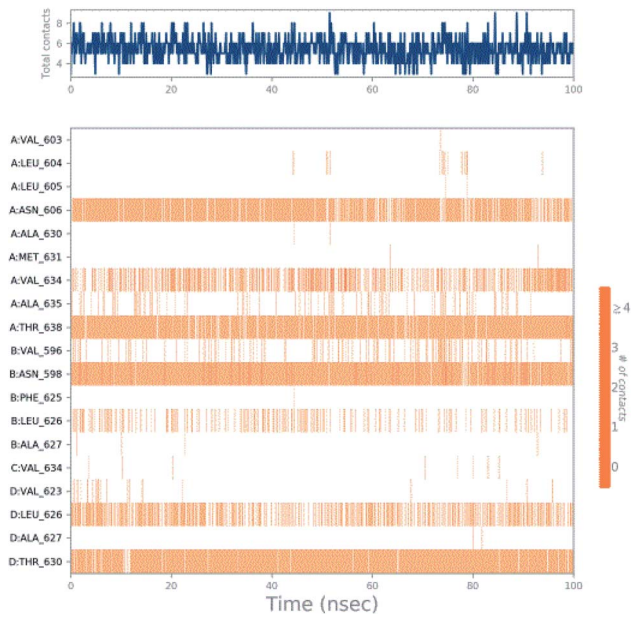

Fig. 8 Timeline representation of ligand–protein contacts for compound **NM28**–5UN1 complex observed during molecular dynamics simulation.

of simulation it attains constant RMSD value. In the beginning, RMSD values of C-alphas, heavy atoms, backbone and side chains are 4.23, 4.24, 4.23 and 4.50 Å, respectively. After MD simulation for 100 ns, we observed average RMSD values of C-alphas (Fig. 6), heavy atoms, backbone and side chains as 9.15, 8.96, 9.12 and 8.98 Å, respectively. **NM28** has RMSD of 3.00 Å at the starting and after simulation it reached to constant value of 6.65 Å. Protein–ligand interactions of all the complexes have been examined during the course of MD simulation. Fig. 7 demonstrates the type of protein–ligand contacts exhibited by all the complexes employed in MD simulation. Mainly, there are three types of protein–ligand interactions: H-bonds, hydrophobic and water bridges. During the course of the MD simulation, H-bond interactions with residues Asn606(A), Thr638(A), Asn598(B) and Thr630(D) were observed, among which more contribution for H-bond interaction fraction was shown by Asn598(B) and Thr630(D). **NM28** has good number of hydrophobic interactions with the active site residues Val634(A), Ala635(A), Leu626(B) and further strong interaction with Leu626(D) during MD simulation. In the results obtained from the MD studies, it was found that the carbonyl oxygen and nitrogen atoms belonging to the amidic groups of the lead analogue **NM28**, showed strong hydrogen bonding with Thr630(D) and Thr638(A) amino acid residues respectively. Similarly, nitrogen and carbonyl oxygen atoms of cycloocta[*b*]pyridine moiety of **NM28** established H-bonds with Asn598(B) and Asn606(A) amino acid residues of the NMDA protein. These interactions strengthen the binding of the molecule at the active binding site, suggesting their potential NMDA inhibitory capability. Fig. 8–10 illustrates timeline representation of ligand–protein contacts including both H-bond and hydrophobic interactions for compound **NM28**, **MK-801** and **HupA** with protein during 100 ns MD simulation period. Further,

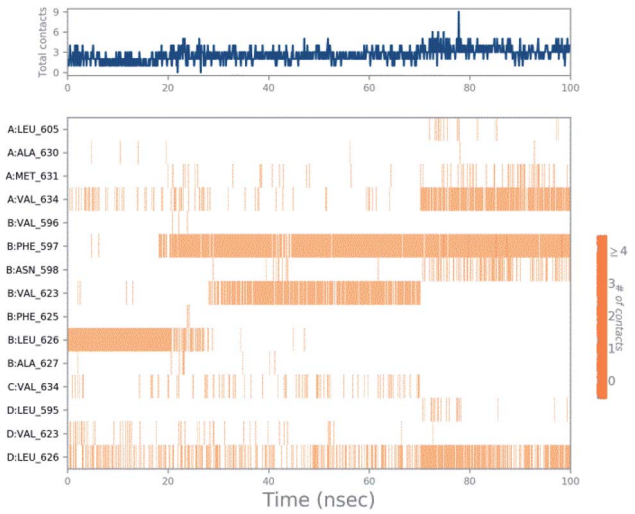

Fig. 9 Timeline representation of ligand–protein contacts for compound MK-801–5UN1 complex observed during molecular dynamics simulation.

ligand–protein interactions of **MK-801**–5UN1 and **HupA**–5UN1 complexes were also analyzed during time period of MD simulation (100 ns). **MK-801** has shown hydrophobic interactions with the residues Met631(A), Val634(A), Val634(C), Val623(D), Leu626(D) and hydrogen bond interaction with Phe597(B), Leu626(B). **HupA** has hydrophobic interactions with Val634(A), Leu626(B), Val623(D), Leu626(D) and hydrogen bond interactions with Asn598(B), Asn599(B) and Leu626(B). In addition, MD studies were also performed on **NM14**, **NM16**, **NM20** and **NM22** to understand their conformational stability at the active pocket

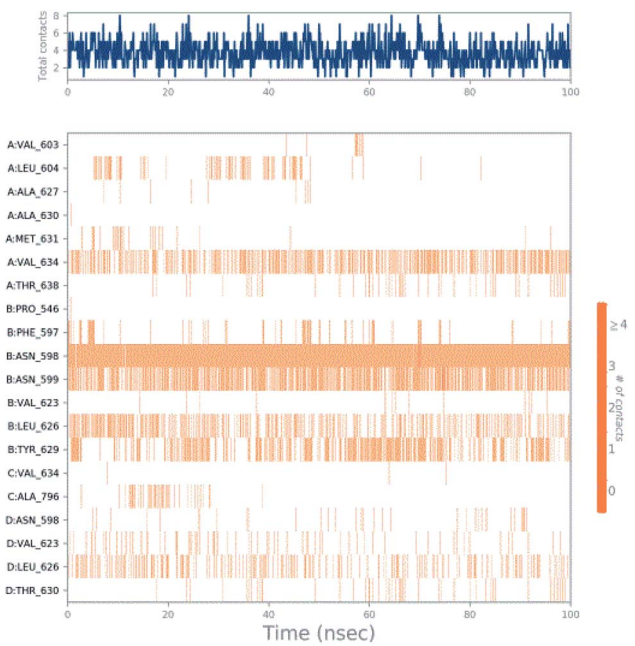

Fig. 10 Timeline representation of ligand–protein contacts for compound HupA–5UN1 complex observed during molecular dynamics simulation.

of NMDA receptor. Fig. S6 and S7 (ESI)† demonstrate the RMSD values and type of protein–ligand contacts exhibited **NM14**, **NM16**, **NM20** and **NM22** with NMDA receptor during 100 ns MD simulation studies. Overall from this MD simulation study, we observed that the compound **NM28** has little fluctuations in the beginning and is more stable at the active site of 5UN1 during course of MD simulation. **NM28** further shows number of favorable contacts with the active site residues that might enhance its binding into the NMDA receptor.

3.3.1 Simulation quality analysis. Further, simulation quality analysis tool of Desmond module was used to analyze the thermodynamic properties which includes energy values with standard deviation was depicted in Tables S3–S5 (ESI).† The tables display valuable information about MD simulation parameters and show the statistical properties of basic thermodynamic quantities. From this analysis, we understood that during the course of MD simulation study, standard deviation become its minimum, it indicates that simulation has equilibrated and its fluctuations was stabilized.

4. Conclusions

The present study marks the beginning of our efforts to obtain more potential NMDA receptor antagonists by exploring the structural behavior and binding affinities of novel **HupA** analogues by molecular docking, ADME/T and molecular dynamics simulation studies for virtual identification of NMDA receptor antagonists. While **NM28** displayed the highest molecular docking score, **NM14**, **NM16**, **NM20**, **NM22** along with **NM28** showed better correlation in terms of binding affinities and interactions. Comparative MD analysis with time period of 100 ns on these lead molecules very well explains the conformational stability and natural dynamics of the interaction in physiological environmental condition. ADME/T prediction on the lead molecules enabled us to analyze their physicochemical and pharmacokinetic profiles. The obtained results will aid in the launch of new research protocols for discovery of potential NMDA receptor antagonists in the treatment of Alzheimer's disease.

Conflicts of interest

There are no conflicts to declare.

Acknowledgements

Authors are thankful to NIPER Hyderabad for facilities and Vinod Devaraji, Schrodinger, Bengaluru for molecular dynamics studies. Authors are also thankful to Dr Sreedhara Voleti, CEO, BioNest, UoH for timely help and advice. DKS thanks Department of Pharmaceuticals (DoP), Govt. of India, New Delhi, for the award of research fellowship.

References

1 H. Hsieh, J. Boehm, C. Sato, T. Iwatsubo, T. Tomita, S. Sisodia and R. Malinow, *Neuron*, 2006, **52**, 831–843.

2 F. Kamenetz, T. Tomita, H. Hsieh, G. Seabrook, D. Borchelt, T. Iwatsubo, S. Sisodia and R. Malinow, *Neuron*, 2003, **37**, 925–937.
3 P. N. Lacor, M. C. Buniel, P. W. Furlow, A. S. Clemente, P. T. Velasco, M. Wood, K. L. Viola and W. L. Klein, *J. Neurosci.*, 2007, **27**, 796–807.
4 M. P. Lambert, A. K. Barlow, B. A. Chromy, C. Edwards, R. Freed, M. Liosatos, T. E. Morgan, I. Rozovsky, B. Trommer, K. L. Viola, P. Wals, C. Zhang, C. E. Finch, G. A. Krafft and W. L. Klein, *Proc. Natl. Acad. Sci. U. S. A.*, 1998, **95**, 6448–6453.
5 G. M. Shankar, B. L. Bloodgood, M. Townsend, D. M. Walsh, D. J. Selkoe and B. L. Sabatini, *J. Neurosci.*, 2007, **27**, 2866–2875.
6 L. Texidó, M. Martín-Satué, E. Alberdi, C. Solsona and C. Matute, *Cell Calcium*, 2011, **49**, 184–190.
7 J. T. Ting, B. G. Kelley, T. J. Lambert, D. G. Cook and J. M. Sullivan, *Proc. Natl. Acad. Sci. U. S. A.*, 2007, **104**, 353–358.
8 D. M. Walsh, I. Klyubin, J. V. Fadeeva, W. K. Cullen, R. Anwyl, M. S. Wolfe, M. J. Rowan and D. J. Selkoe, *Nature*, 2002, **416**, 535–539.
9 H. W. Wang, J. F. Pasternak, H. Kuo, H. Ristic, M. P. Lambert, B. Chromy, K. L. Viola, W. L. Klein, W. B. Stine, G. A. Krafft and B. L. Trommer, *Brain Res.*, 2002, **924**, 133–140.
10 N. W. Hu, I. Klyubin, R. Anwyl and M. J. Rowan, *Proc. Natl. Acad. Sci. U. S. A.*, 2009, **106**, 20504–20509.
11 S. Li, M. Jin, T. Koeglsperger, N. E. Shepardson, G. M. Shankar and D. J. Selkoe, *J. Neurosci.*, 2011, **31**, 6627–6638.
12 J. Liu, L. Chang, F. Roselli, O. F. Almeida, X. Gao, X. Wang, D. T. Yew and Y. Wu, *J. Alzheimer's Dis.*, 2010, **22**, 541–556.
13 G. Rammes, A. Hasenjäger, K. Sroka-Saidi, J. M. Deussing and C. G. Parsons, *Neuropharmacology*, 2011, **60**, 982–990.
14 R. Rönicke, M. Mikhaylova, S. Rönicke, J. Meinhardt, U. H. Schröder, M. Fändrich, G. Reiser, M. R. Kreutz and K. G. Reymann, *Neurobiol. Aging*, 2011, **32**, 2219–2228.
15 F. Roselli, P. Hutzler, Y. Wegerich, P. Livrea and O. F. Almeida, *PLoS One*, 2009, **4**, e6011.
16 P. Paoletti, C. Bellone and Q. Zhou, *Nat. Rev. Neurosci.*, 2013, **14**, 383–400.
17 A. Barria and R. Malinow, *Neuron*, 2002, **35**, 345–353.
18 K. Erkan, S. Noriko and F. Hiro, *EMBO J.*, 2009, **28**, 3910–3920.
19 P. K. Alan and T. Werner, *Acc. Chem. Res.*, 1999, **32**, 641–650.
20 K. G. Richard, V. N. Savita, A. W. Julie, R. D. Jitendra, P. D. Bhupendra and S. V. Haresh, *J. Appl. Toxicol.*, 2001, **21**, S47–S51.
21 H. Z. Yun, Y. Z. Xiao, Q. C. Xue, W. Yuan, H. Y. Hui and Y. H. Guo, *Neurosci. Lett.*, 2002, **319**, 107–110.
22 H. Gunosewoyo, S. K. Tipparaju, M. Pieroni, Y. Wang, B. P. Doctor, M. P. Nambiar and A. P. Kozikowski, *Bioorg. Med. Chem. Lett.*, 2013, **23**, 1544–1547.
23 P. K. Alan, X. Yan, R. E. Rajarathnam, T. Werner, H. Israel and X. C. Tang, *J. Org. Chem.*, 1991, **56**, 4636–4645.
24 C. Pelayo, M. Diego and S. Montserrat, *Synth. Commun.*, 2001, **31**, 3507–3516.
25 A. K. Seán, F. Yann, M. John and M. B. Jonathan, *Org. Biomol. Chem.*, 2003, **1**, 2865–2876.
26 S. Kaneko, T. Yoshino, T. Katoh and S. Terashima, *Tetrahedron: Asymmetry*, 1997, **8**, 829–832.
27 S. Kaneko, T. Yoshino, T. Katoh and S. Terashima, *Tetrahedron*, 1998, **54**, 5471–5484.
28 X. C. He, B. Wang and D. Bai, *Tetrahedron Lett.*, 1998, **39**, 411–414.
29 X. C. He, B. Wang, G. Yu and D. Bai, *Tetrahedron: Asymmetry*, 2001, **12**, 3213–3216.
30 X. Song, M. O. Jensen, V. Jogini, R. A. Stein, C. H. Lee, H. S. Mchaourab, D. E. Shaw and E. Gouaux, *Nature*, 2018, **556**, 515–519.
31 *Maestro (Version 11.1)*, Schrödinger, LLC, New York, NY, 2017.
32 G. M. Sastry, M. Adzhigirey, T. Day, R. Annabhimoju and W. Sherman, *J. Comput. Aided Mol. Des.*, 2013, **27**, 221–234.
33 *Schrödinger Release 2017-1: Schrödinger Suite 2017, Protein Preparation Wizard; Epik (Version 3.9)*, Schrödinger, LLC, New York, NY, 2017; *Impact (Version 7.4)*, Schrödinger, LLC, New York, NY,2017.
34 T. Halgren, *Chem. Biol. Drug Des.*, 2007, **69**, 146–148.
35 T. Halgren, *J. Chem. Inf. Model.*, 2009, **49**, 377–389.
36 *LigPrep*, Schrödinger, LLC, New York, NY, 2017.
37 R. A. Friesner, J. L. Banks, R. B. Murphy, T. A. Halgren, J. J. Klicic, D. T. Mainz, M. P. Repasky, E. H. Knoll, D. E. Shaw, M. Shelley, J. K. Perry, P. Francis and P. S. Shenkin, *J. Med. Chem.*, 2004, **47**, 1739–1749.
38 *GLIDE (Version 7.4)*, Schrödinger, LLC, New York, NY, 2017.
39 W. L. DeLano, *PyMOL*, DeLano Scientific, San Carlos, CA, 700, 2002.
40 *Qikprop (Version 5.1)*, Schrödinger, LLC, New York, NY, 2017.
41 *Desmond (Version 4.9)*, Schrödinger, LLC, New York, NY, 2017.